Scripta Materialia 130 (2017) 100–104

Contents lists available at ScienceDirect

Scripta Materialia

journal homepage: www.elsevier.com/locate/scriptamat

Regular Article

Intrinsic size effect of CuTa/Cu nanolaminates with unequal modulation ratios

C Gu [a], P Huang [a,*], M B Liu [b], K W Xu [a], F Wang [b,*], T J Lu [b,c]

[a] State-Key Laboratory for Mechanical Behavior of Material, Xi'an Jiaotong University, Xi'an 710049, China
[b] State Key Laboratory for Strength and Vibration of Mechanical Structures, School of Aerospace, Xi'an Jiaotong University, Xi'an 710049, China
[c] MOE Key Laboratory for Multifunctional Materials and Structures, Xi'an Jiaotong University, Xi'an 710049, China

ARTICLE INFO

Article history:
Received 9 October 2016
Received in revised form 20 November 2016
Accepted 20 November 2016
Available online 30 November 2016

Keywords:
Amorphous
Interface
Shear band
Nanoindentation
Size effect

ABSTRACT

In order to study the intrinsic size effect of nanolaminates with unequal modulation ratios, CuTa/Cu nanolaminates with identical Cu layer volume fraction but different Cu layer thicknesses were prepared by varying the number of Cu layers. The hardness and indentation morphology of each CuTa/Cu nanolaminate was characterized by means of nanoindentation and scanning electron microscope. Furthermore, the microstructures of CuTa/Cu nanolaminates with different interfacial configurations were examined under high resolution transmission electron microscopy. The deformation of CuTa/Cu nanolaminates was found to be dominated by the thickness ratio between CuTa and Cu layers as well as the interfacial microstructure.

Amorphous materials attracted increased attention due to their fundamental scientific importance and engineering application potential [1,2]. However, the application of amorphous thin films is seriously limited by nearly zero plasticity due to catastrophic failure caused by shear bands (SBs) formation and propagation [2]. An effective way to enhance the mechanical properties of amorphous materials was to introduce crystalline layers into monolayer amorphous thin film, forming the amorphous/crystalline (A/C) nanolaminate structure [3]. The deformation mechanism of A/C nanolaminate was found to be strongly size dependent, because the formation or propagation of SBs in amorphous layer and dislocation motion in crystalline layer were both size dependent [4–6]. Existing research on A/C nanolaminates mainly focused on structures with unequal modulation ratios [7–9], as A/C nanolaminates with equal modulation ratios exhibited the worst plasticity behavior [10]. Traditionally, to investigate the size effect of A/C nanolaminates with unequal modulation ratios, the thickness of amorphous or crystalline layer was fixed while the thickness of the other layer was altered [7,8], or the modulation wavelength was fixed while the modulation ratio was varied [10]. For these structures, the volume fraction of both C layer and A layer changed when individual layer thickness in A/C nanolaminate was altered. Under such conditions, although the mechanical properties of the nanolaminate changes with varying layer thickness, it also changes with varying volume fraction of the two constituent layers. That is, the hardness would be affected by both the size-dependent strengthening mechanism and the volume fraction factor. This additional volume fraction factor would also affect the plasticity of the system as the plasticity might be improved by increasing the volume fraction of ductile constituent layers. As a result, it was hard to clarify whether the change of mechanical properties was mainly caused by the size factor or by volume fraction factor. And the question arises as what is the real size effect without the influence of volume fraction factor, i.e., the intrinsic size effect, in nanolaminate systems with unequal modulation ratios. In order to investigate the intrinsic size effect of A/C nanolaminates, the volume fraction of both the crystalline layer and the amorphous layer should be kept constant.

In the present study, series of CuTa/Cu A/C nanolaminates with fixed Cu layer volume fraction were prepared. While discussing the size-dependent deformation mechanism, the thickness of Cu layer and CuTa layer in each series of A/C nanolaminates was varied by varying the number of Cu layers. Furthermore, by varying the volume fraction of Cu layer in two different series of samples, the size effect of CuTa/Cu nanolaminates having identical Cu layer thickness but different Cu layer volume fractions were also discussed. In addition, by controlling the Ta content in CuTa layer, CuTa/Cu nanolaminates having identical structural configuration but different interfacial structures were prepared. The effect of interfacial structure on the deformation mechanisms of these samples was analyzed.

CuTa monolayers and CuTa/Cu nanolaminates were deposited on Si(100) wafers by magnetron sputtering. CuTa monolayers were deposited using the pure Cu and Ta targets co-sputtering mode, which were

* Corresponding authors.
E-mail addresses: huangping@mail.xjtu.edu.cn (P. Huang), wangfei@mail.xjtu.edu.cn (F. Wang).

http://dx.doi.org/10.1016/j.scriptamat.2016.11.026
1359-6462/

connected with radio frequency (RF) power and direct current (DC) power, respectively. During deposition, the RF power was fixed at 100 W while the DC power was fixed at 60 W and 80 W, respectively, so as to obtain two CuTa monolayers with different Ta contents. Energy disperse spectroscopy (EDS) results showed that the Ta content of the CuTa monolayer deposited with a DC power of 60 W and 80 W was separately 34 at.% and 42 at.% (denoted below as CuTa34 and CuTa42). Subsequently, by depositing alternatively the CuTa layer and the Cu layer, CuTa/Cu nanolaminates were prepared. Specifically, samples of CuTa34/Cu and CuTa42/Cu with Cu layer thickness of 50 nm, 20 nm, 10 nm and 5 nm were prepared by fixing the Cu layers volume fraction at 1/15 (i.e., the total thickness of Cu layers was 100 nm) and varying the number of Cu layers as 2, 5, 10 and 20, respectively. Further, the volume fraction of Cu layers was set as 2/15 for CuTa34/Cu, i.e., the total thickness of Cu layers was 200 nm. Again, with the number of Cu layers varied as 2, 5, 10 and 20, the Cu layer thickness became 100 nm, 40 nm, 20 nm and 10 nm. For both CuTa monolayers and CuTa/Cu nanolaminates, the total thickness was fixed at 1.5 μm.

The microstructural features of CuTa monolayers and CuTa/Cu nanolaminates were investigated by examining their cross-sectional images under high-resolution transmission electron microscopy (HRTEM, JEOL JEM-2100F operating at 200 KV). Nanoindentation tests were carried out using a MTS Nanoindenter XP system (MTS, Inc.) under Continuous Stiffness Measurement (CSM) mode. Berkovich indenter was chosen to measure the hardness of all samples. The indentation depth was 200 nm and 1500 nm (i.e., equal to layer thickness) for hardness test and residual indentation morphology examination, respectively. In each test, a total of 12 indents were performed, with the applied strain rate fixed at 0.05 s^{-1}.

The inset of Fig. 1(a) illustrated schematically the present CuTa/Cu nanolaminates: the thickness of Cu layers varied with the number of Cu layers by fixing the volume fraction of Cu layers in the nanolaminates. Fig. 1(a) and (c) presented nanoindentation hardness results for all the nanolaminates. Two series of CuTa/Cu nanolaminates were compared: series I had identical Cu layer and CuTa layer microstructures but different Cu layer volume fractions while series II had the same Cu layer thickness and Cu layer volume fraction but different interfacial structures.

Fig. 1(a) plotted the hardness of CuTa34/Cu as a function of Cu layer thickness for series I, where the total Cu layer thickness for CuTa/Cu-100 and CuTa/Cu-200 was 100 nm and 200 nm, respectively. For CuTa34/Cu-100, the hardness increased with increasing Cu layer thickness. In contrast, For CuTa34/Cu-200, the hardness decreased with increasing Cu layer thickness. This quite different variation trend of hardness between these two groups of samples indicated that the two sample groups possessed different deformation mechanisms even when they had identical Cu layer thickness.

The hardness of A/C nanolaminate system was considered to be affected synthetically by the crystalline layer, the amorphous layer and the interface. A simple relationship of rule of mixture always used to reveal the underlying deformation mechanism of the nanolaminate structure [3,4,7]. The hardness of present CuTa/Cu samples calculated by the rule of mixture, H_{ROM}, was given by:

$$H_{ROM} = H_{CuTa} \cdot f_{CuTa} + H_{Cu} \cdot f_{Cu} \quad (1)$$

where H_{CuTa} and H_{Cu} were the hardness of CuTa layer and Cu layer, and f_{CuTa} and f_{Cu} were the volume fraction of CuTa layer and Cu layer, respectively. In previous studies, amorphous materials were found to be size-independent over a wide range of samples sizes [11–14]. As a result, H_{CuTa} should be constant in Eq. (1). However, the crystalline layer exhibited distinct size effect [15–17]. To confirm the size-dependent strengthening mechanism of Cu layer, the TEM images of CuTa34/Cu were examined as shown in Fig. 2(a)–(c). From the selected area electron diffraction (SAED) pattern of CuTa34/Cu-100(5) shown in Fig. 2(a), both amorphous halo and crystalline diffraction spots could be

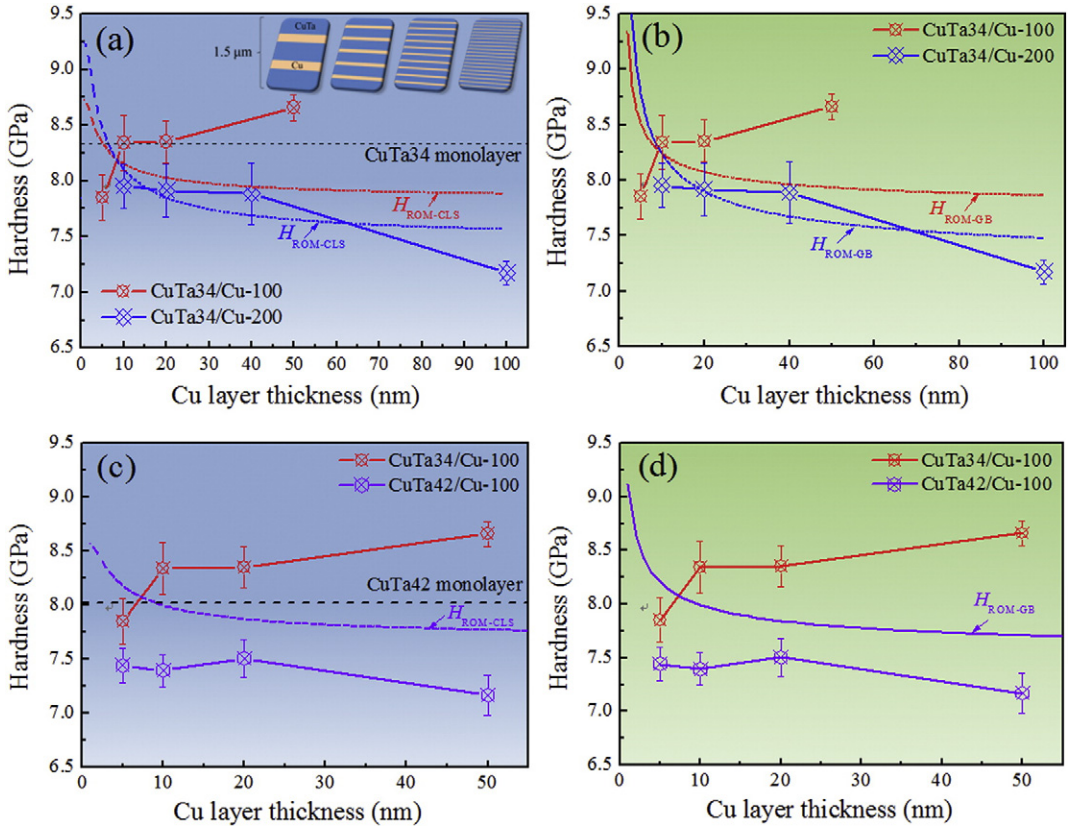

Fig. 1. (a) and (b) nanoindentation hardness of CuTa34/Cu-100 compared with that of CuTa34/Cu-200, the inset of (a) presented the schematic illustration of CuTa/Cu nanolaminates, (c) and (d) nanoindentation hardness of CuTa34/Cu compared with that of CuTa42/Cu.

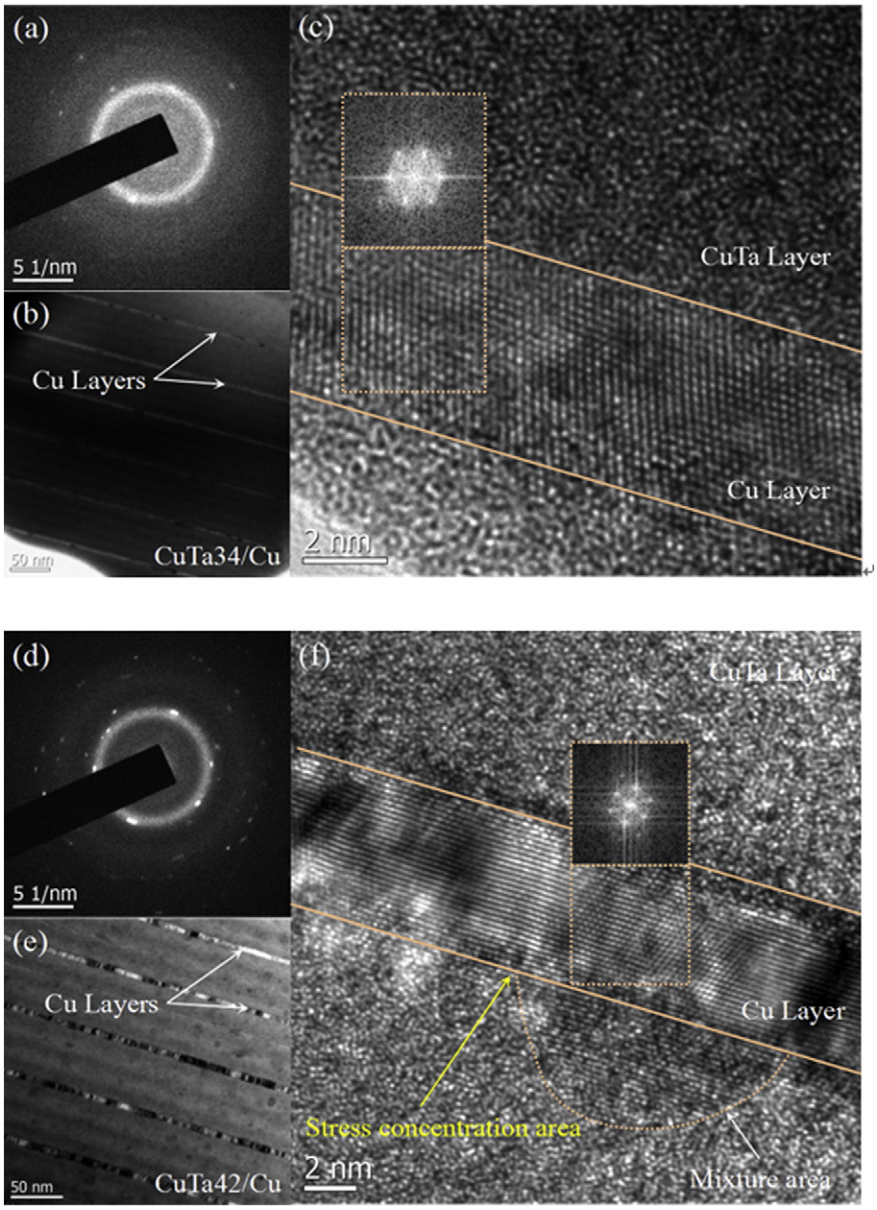

Fig. 2. HRTEM images: (a)–(c) CuTa34/Cu and (d)–(f) CuTa42/Cu.

observed. Here, for brevity, a test sample with a single Cu layer thickness of x nm was denoted as CuTa/Cu(x). From the bright field image of the sample shown in Fig. 2(b), it was seen that the Cu layers were evenly distributed in the CuTa amorphous matrix, and the CuTa-Cu interface was clear and straight. More detailed microstructures of Cu layer and CuTa-Cu interface were presented in the HRTEM image of Fig. 2(c): atoms in the Cu layer were seen to have regularly textured growth. The fast Fourier transform (FFT) of Cu layer shown in the insert of Fig. 2(c) indicated that Cu(111) had plan growth parallel to CuTa-Cu interface. For crystalline/crystalline nanolaminates with individual layer thickness less than 100 nm, it had been demonstrated that the confined layer slip (CLS) model could predict the experimental results well [5]. For a single dislocation slipping in a confined layer, the structural condition of the present Cu layer was the same as that of crystalline/crystalline nanolaminates. Consequently, the hardness of Cu layer was calculated using the CLS model as [5]:

$$\sigma_{CLS} = M\frac{\mu^* b}{8\pi h'}\left(\frac{4-\nu}{1-\nu}\right)\ln\frac{\alpha h'}{b} - \frac{f}{h} + \frac{\mu^* b}{L(1-\nu)} \tag{2}$$

According to existing molecular dynamics (MD) simulation results [18], amorphous-crystalline interfaces (ACIs) acted as dislocation sink and source, similar to the role of grain boundaries in nanocrystalline metals. The results of analytical models [19,20] based on dislocation theory indicated that the resolved shear stress for partial dislocations emission was lower than that for full dislocations when the grain size was less than 50 nm. As most of the present nanolaminate systems had a Cu layer thicknesses less than 50 nm, the resolved shear stress of Cu layer was also predicted using the model for partial dislocations emission and denoted below as H_{GB}. The resolved shear stress at which a partial dislocation was emitted from GBs could be calculated as [19]:

$$\frac{\tau}{G} = \zeta\sqrt{\frac{b^{(1)}}{d}} \tag{3}$$

where G was the shear modulus, $\zeta = 0.251$ for Cu, $b^{(1)} = b/\sqrt{3}$ and d was the grain size (or Cu layer thickness in the present study).

By substituting the parameters taken from [7,19] into Eqs. (2) and (3) and fixing H_{CuTa} as a constant, the prediction lines of H_{ROM} for the present CuTa/Cu nanolaminates were added to Fig. 1(a) and (b), with the calculated values converted via $H = 2.7\sigma$ and $\sigma = 3.1\tau$. The red dashed lines were predictions for CuTa34/Cu-100 with a fixed Cu layer volume fraction of 1/15, while the blue dashed lines were predictions for CuTa34/Cu-200 with a fixed Cu layer volume fraction of 2/15. For CuTa34/Cu-200, $H_{ROM\text{-}CLS}$ predicted the experimental data much better than $H_{ROM\text{-}GB}$. The consistency of hardness values between those calculated by ROM and measured experimentally indicated a weak ACI effect in CuTa34/Cu-200. The result also indicated that the deformation mechanism of CuTa34/Cu-200 was strongly dependent upon the size effect of Cu layers and the dislocation mode was single dislocation slipping in confined Cu layer rather than emission from ACI and passing through the Cu layer. This mechanism of dislocation slipped in confined Cu layer was also proved in a CuZr/Cu system with CuZr layer thickness of 100 nm and Cu layer thickness of 50 nm [7]. As a visually impression that reflected the deformation behavior, indentation morphologies of present CuTa/Cu samples were also examined under scanning electron microscope (SEM) as shown in Fig. 3. According to Fig. 3(a)–(d), CuTa34/Cu-200 exhibited nearly identical indentation morphologies for samples with the Cu layer thickness varying from 100 nm to 10 nm. Consequently, the deformation mechanism of all the CuTa34/Cu-200 samples would not change as the Cu layer thickness was varied.

For CuTa34/Cu-100, the hardness variation trend was quite different from CuTa34/Cu-200 and both $H_{ROM\text{-}CLS}$ and $H_{ROM\text{-}GB}$ failed to predict the experimental results. Relative to CuTa34/Cu-200, the totally opposite hardness variation trend of CuTa34/Cu-100, i.e., smaller was weaker, indicated a pronounced ACI effect. Dislocations were considered to be emitted from one ACI and absorbed by the opposite ACI rather than slipping in the confined layer. Such dislocation motion could be proved, to some extent, by the close match between $H_{ROM\text{-}GB}$ and experimental results for CuTa34/Cu-100(10) and CuTa34/Cu-100(20) as shown in Fig. 1(b). However, the hardness of CuTa34/Cu-100(5) was lower than both $H_{ROM\text{-}GB}$ and monolayer CuTa. Greer et al. [21] found that the deformation process of metallic glass pillars was transformed from SB nucleation controlled to SB propagation controlled as the pillar diameter was reduced. As shown schematically in Fig. 4, although the critical stress for SB nucleation was low, additional stress was needed for the propagation of SB so that a higher stress was needed for 1.5 μm thick CuTa thin films. However, the stress for SB nucleation became extremely high when the amorphous layer thickness was reduced to a relative small value such as area 1 in Fig. 4. For CuTa34/Cu-100(5), dislocations could be activated from ACI under the applied stress and then be absorbed by the opposite ACI. The absorption of dislocations would trigger the movement of STZs near the ACI [18]. However, since STZs could not develop into SB due to the high SB nucleation stress, stress concentration would occur near the triggered STZs area. As the nucleation and coalescence of STZs reduced the flow stress [22] for BMGs, cracks would easily initialize in the STZ accumulation area (where atoms arrangement was loose) and then propagate along the shear plane due to stress concentration. Consequently, the strength of CuTa34/Cu(5) decreased.

For CuTa34/Cu-100(10) and CuTa34/Cu-100(20), STZs could also be triggered near the ACI due to dislocations absorption. However, as shown in Fig. 4, the stress for SB nucleation in either area 2 or area 3 was lower than that in area 1, so that the nucleation and propagation of SBs caused the reduction in system energy: as a result, no stress concentration occurred near the ACI. Previously, it was found that the deformation behavior of metallic glasses would transform from inhomogeneous to homogeneous when the critical diameter of 1 μm was reached in compression tests [21]. As the thickness of CuTa layer was smaller than 1 μm for all the samples tested in the present study, homogeneous deformation was considered to occur in the CuTa layer. As an obvious characteristic of homogeneous deformation in amorphous materials was the formation and interaction of multiple SBs [13,22,23], the interaction of SBs would enhance the strength of nanolaminates. For CuTa34/Cu-100(10) and CuTa34/Cu-100(20), limited dislocations were activated from ACI due to the small Cu layer thickness [6]. Consequently, few SBs were formed near the ACI, resulting in weak SBs interaction strengthening relative to monolayer CuTa. For CuTa34/Cu-100(50), the pronounced strengthening effect was mainly attributed to enhanced SBs interaction due to continuous dislocation emission and SBs nucleation. As the interaction of SBs would inhibit mature SB propagation, the SBs density in CuTa34/Cu-100(50) was lower than other systems as shown in Fig. 3(e)–(h).

According to the foregoing discussion, samples with same Cu layer thickness but different Cu layer volume fraction, such as CuTa34/Cu-100(10) and CuTa34/Cu-200(10), presented different hardness values and deformation mechanisms. The thickness ratio between CuTa and Cu layers, η, was further examined here. For CuTa34/Cu-100, η had a value of 9.3, 11.7, 12.7 and 13.4, corresponding to a Cu layer thickness of 50 nm, 20 nm, 10 nm and 5 nm. For CuTa34/Cu-200, the value of η was 4.3, 5.4, 5.9 and 6.2, corresponding to a Cu layer thickness of 100 nm, 40 nm, 20 nm and 10 nm. These results suggested that the value of η for CuTa34/Cu-200 was much smaller than that of CuTa34/Cu-100. Even if CuTa34/Cu-100(10) and CuTa34/Cu-200(10) had the same Cu layer thickness of 10 nm, the difference in their η values would cause different deformation mechanisms. In general, in the present study, the deformation mechanism was dominated by the CLS type ROM when η was relatively low and by the ACI when η was relatively large. While a slightly change in volume fraction would cause an obvious difference in η, and then further affected the deformation behavior,

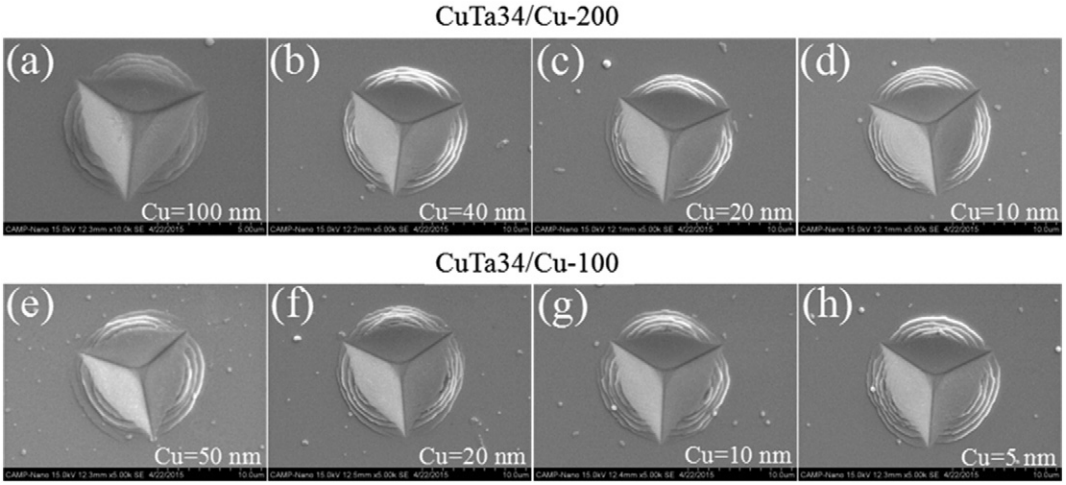

Fig. 3. Nanoindentation morphologies: (a)–(d) CuTa34/Cu-200 and (e)–(h) CuTa34/Cu-100.

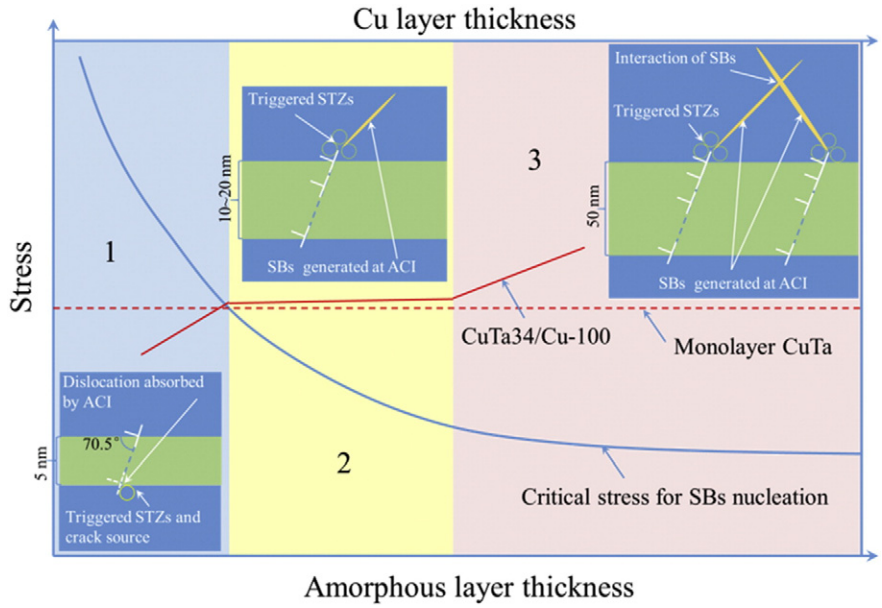

Fig. 4. Schematic of deformation mechanism for CuTa34/Cu-100.

the intrinsic size-dependent deformation mechanism was greatly weakened in the previous nanolaminate systems with unequal modulation ratios. Consequently, the size-dependent deformation mechanism could hardly get a universal application in different nanolaminate systems with unequal modulation ratios.

As the ACI played an important role in the deformation mechanism of CuTa34/Cu-100, samples (i.e., series II) with identical layer thickness but different ACI structures were prepared to further investigate the effect of ACI. The results were presented in Fig. 1(c) and (d), with the hardness of CuTa34/Cu-100 and CuTa42/Cu-100 plotted as a function of Cu layer thickness. For CuTa34/Cu-100, the hardness was in general larger than CuTa34 except for CuTa34/Cu-100(5). However, for all the samples shown in Fig. 1(c), the hardness of CuTa42/Cu-100 was lower than monolayer CuTa42. Again, both $H_{ROM\text{-}CLS}$ and $H_{ROM\text{-}GB}$ failed to predict the hardness variation trend of CuTa42/Cu-100.

Fig. 2(d)–(f) showed the TEM image of CuTa42/Cu-100. The SAED pattern and bright field image shown separately in Fig. 2(d) and (e) were both similar to those of CuTa34/Cu-100. The FFT image shown in the insert of Fig. 3(f) indicated that the Cu layer structure of CuTa42/Cu-100 was identical to that of CuTa34/Cu-100. However, the HRTEM image shown in Fig. 3(f) demonstrated that the interfacial structure of CuTa42/Cu-100 was quite different from that of CuTa34/Cu-100. Between the Cu layer and the CuTa layer of CuTa42/Cu-100, a mixture area was present within which the arrangement of atoms was crystalline like. During nanoindentation, stress concentration would occur near the interface between ACI and the mixture area, as marked by the yellow arrow in Fig. 2(f). Such stress concentration could act as the nucleation source for SBs, where the stress needed for SB nucleation was decreased. As a result, the hardness of CuTa42/Cu-100 was much lower than that of CuTa42 and remained nearly constant.

In summary, two series of CuTa/Cu nanolaminate systems were prepared. For series I, Cu layers with a total thickness of 100 nm or 200 nm were evenly added into the 1.5 μm thick CuTa34 amorphous matrix. Nanoindentation results indicated that the deformation mechanism was strongly dependent upon the thickness ratio η between CuTa and Cu layers. For relatively small η values, the hardness could be predicted well by the CLS mode ROM. For higher η values, ACI played an important role in the dominant deformation mechanism. The results revealed why does the size-dependent deformation mechanism has little universality in different nanolaminate systems according to existing research. In is also indicated that the performance of a nanolaminate may be optimized by controlling the η value and varying the layer thickness, other than playing with the single parameter of layer thickness as in nanolaminates with equal modulation ratios. For series II, samples with identical layer thickness but different interfacial structures were prepared. The results demonstrated that the structure of ACI was another important factor affecting the size effect of C/A nanolaminates. Results of the present study revealed that pure ACI caused a strengthening effect while ACI with a mixture area caused a softening effect.

Acknowledgements

The present work was supported by the National Natural Science Foundation of China (51171141, 51271141, and 51471131).

References

[1] W.H. Wang, C. Dong, C.H. Shek, Mater. Sci. Eng. R 44 (2004) 45–89.
[2] C. Schuh, T. Hufnagel, U. Ramamurty, Acta Mater. 55 (2007) 4067–4109.
[3] J.Y. Kim, D. Jang, J.R. Greer, Adv. Funct. Mater. 21 (2011) 4550–4554.
[4] A. Donohue, F. Spaepen, R.G. Hoagland, A. Misra, Appl. Phys. Lett. 91 (241905) (2007) 6.
[5] A. Misra, J.P. Hirth, R.G. Hoagland, Acta Mater. 53 (2005) 4817–4824.
[6] L. Fang, L.H. Friedman, Philos. Mag. 85 (2005) 3321–3355.
[7] W. Guo, E. Jägle, J. Yao, V. Maier, S. Korte-Kerzel, J.M. Schneider, D. Raabe, Acta Mater. 80 (2014) 94–106.
[8] W. Guo, B. Gan, J.M. Molina-Aldareguia, J.D. Poplawsky, D. Raabe, Scr. Mater. 110 (2016) 28–32.
[9] I. Knorr, N.M. Cordero, E.T. Lilleodden, C.A. Volkert, Acta Mater. 61 (2013) 4984–4995.
[10] Y.Q. Wang, J.Y. Zhang, X.Q. Liang, K. Wu, G. Liu, J. Sun, Acta Mater. 95 (2015) 132–144.
[11] C.A. Volkert, A. Donohue, F. Spaepen, J. Appl. Physiol. 103 (2008) 083539.
[12] X. Wang, F. Jiang, H. Hahn, J. Li, H. Gleiter, J. Sun, J. Fang, Scr. Mater. 116 (2016) 95–99.
[13] C.Q. Chen, Y.T. Pei, J.T.M. De Hosson, Acta Mater. 58 (2010) 189–200.
[14] M. Ghidelli, S. Gravier, J.J. Blandin, P. Djemia, F. Mompiou, G. Abadias, J.P. Raskin, T. Pardoen, Acta Mater. 90 (2015) 232–241.
[15] J.Y. Zhang, G. Liu, S.Y. Lei, J.J. Niu, J. Sun, Acta Mater. 60 (2012) 7183–7196.
[16] J.J. Niu, J.Y. Zhang, G. Liu, P. Zhang, S.Y. Lei, G.J. Zhang, J. Sun, Acta Mater. 60 (2012) 3677–3689.
[17] Q. Zhou, J.Y. Xie, F. Wang, P. Huang, K.W. Xu, T.J. Lu, Acta Mech. Sinica 31 (2015) 319–337.
[18] Y. Wang, J. Li, A.V. Hamza, T.W. Barbee Jr., PNAS 104 (2007) 11155–11160.
[19] R.J. Asaro, S. Suresh, Acta Mater. 53 (2005) 3369–3382.
[20] R.J. Asaro, P. Krysl, B. Kad, Philos. Mag. Lett. 83 (2003) 733–743.
[21] J.R. Greer, J.T.M. De Hosson, Prog. Mater. Sci. 56 (2011) 654–724.
[22] Y. Chen, M.Q. Jiang, L.H. Dai, Int. J. Plast. 50 (2013) 18–36.
[23] J.T. De Hosson, Microsc. Res. Tech. 72 (2009) 250–260.